

RESEARCH ARTICLE

The role of collision and coalescence on the microphysics of marine fog

Camilo F. Rodriguez-Geno  | David H. Richter 

Department of Civil and Environmental Engineering and Earth Sciences, University of Notre Dame, Notre Dame, Indiana

Correspondence

Camilo F. Rodriguez-Geno, Department of Civil and Environmental Engineering and Earth Sciences, University of Notre Dame, Notre Dame, IN 46556, USA.
Email: crodris25@nd.edu

Funding information

Office of Naval Research, Grant/Award Numbers: N00014-21-1-2296, N00014-18-1-2472

Cloud microphysics fulfills a fundamental role in the formation and evolution of marine fog, but it is not fully understood. Numerous studies have addressed this by means of direct observations and modeling efforts. However, collision–coalescence of aerosols and fog droplets is a process often neglected. In this study we perform an analysis of the role of particle collections on the formation, development, and microphysical structure of marine fog. It was found that collisions open a path for aerosol activation by means of collisional activation. In addition, collisions contribute to the diffusional activation of fog particles by adding water mass to the growing aerosols, making them reach the required critical radius faster. Furthermore, collisions have a homogenizing effect on hygroscopicity, facilitating the activation of accumulation-mode aerosols by increasing their diffusional growth.

KEYWORDS

collision–coalescence, collisional activation, fog microphysics, Lagrangian cloud modeling, marine fog, superdroplet method

1 | INTRODUCTION

Marine fog is a common meteorological phenomenon that occurs around the world. It has significant impacts on the environment, climate, and human activities, particularly in coastal regions, where it can cause reduced visibility, economic losses, and transportation disruptions (Gultepe *et al.*, 2007). Understanding the dynamics of marine fog is therefore crucial for developing accurate predictions and mitigation strategies. Furthermore, despite recent advances in atmospheric science, marine fog forecasting remains a highly difficult task because of the sheer number of processes that take place during the fog life cycle and their interactions, with radiative, physical, and chemical being just a few (Gultepe *et al.*, 2017; Mazoyer *et al.*, 2017).

Many of these processes have been thoroughly characterized either by observations and/or numerical modeling (Boutle *et al.*, 2022; Chisholm *et al.*, 2021; Gultepe *et al.*, 2021; Mazoyer *et al.*, 2017; Schwenkel &

Maronga, 2019; Wainwright *et al.*, 2021). In particular, microphysical processes are of great importance, ranging from aerosol composition, nucleation, particle growth by water vapor diffusion, and particles' interactions (Boutle *et al.*, 2022; Koračin *et al.*, 2014). Here, we are specifically concerned with collision–coalescence as a potentially vital component in fog microphysics. This process, despite being a ubiquitous feature of cloud microphysics, is difficult to discern from direct observations, and most experimental studies associated with collision and coalescence have been done under limited laboratory conditions (Low and List, 1982; Barros *et al.*, 2008). This makes numerical modeling an attractive tool to study its effects (Berry, 1967; Berry and Reinhardt, 1974; Bott, 1998; Clark & Hall, 1983; Dziekan & Pawlowska, 2017).

Despite its known importance in clouds, collision and coalescence are considered of secondary importance in fog formation, development, and dissipation (Boutle *et al.*, 2022; Schwenkel & Maronga, 2020), compared with other processes like turbulence, radiation, or

dynamical processes. As a result of this, collision and coalescence are often neglected in fog modeling studies (Schwenkel & Maronga, 2020). However, particle collisions almost certainly take place inside a fog layer, potentially influencing its development. In the later stages of fog life cycle, droplet collisions enhance sedimentation, which in turn widens the droplet size distribution (DSD) (Gultepe *et al.*, 2017). Also, and to the best of our knowledge, there are no previous studies that quantify the effect of particle collisions in the formation stage of fog, either by modifying the shape of the aerosol size distribution (ASD) or by playing a role in aerosol activation. This latter effect has been shown to be possible in stratocumulus clouds, through the so-called “collisional activation” process (Hoffmann, 2017), which raises a number of questions about the role of particle collisions in fog formation.

We therefore hypothesize that the combined effect of aerosol activation, condensation growth, and coalescence (via collisional activation) should be considered when simulating fog events. Hence, the objective of this study is to objectively explain and quantify the role of collision and coalescence of particles (aerosol and droplets) in fog formation. To achieve this, numerical modeling has emerged as a useful tool for studying marine fog (Chen *et al.*, 2021; Dimitrova *et al.*, 2021; Koračin *et al.*, 2014; Richter *et al.*, 2021; Wainwright *et al.*, 2021), and Lagrangian cloud models (LCMs) have been shown to be particularly effective in simulating the microphysical properties of fog droplets (Richter *et al.*, 2021; Schwenkel & Maronga, 2020).

LCMs are based on the assumption that a cloud or fog layer is made up of a large number of individual droplets or particles that move independently of one another. These models simulate the motion and behavior of these individual droplets or particles, providing a more detailed and accurate representation of the processes that occur within the cloud or fog. The superdroplet (SD) method (SDM) has gained popularity in recent years owing to its ability to simulate the full range of droplet sizes and accurately model the microphysical processes that govern the formation and evolution of fog droplets (Morrison *et al.*, 2020; Shima *et al.*, 2009). It works by representing cloud particles as collections of small droplets or SDs, each of which is assumed to have the same properties (mass, hygroscopicity, speed, and so on). These SDs are then tracked individually as they interact with each other and with the surrounding air, allowing the model to capture complex phenomena within clouds (Grabowski *et al.*, 2019; Shima *et al.*, 2009). This approach also allows for a seamless implementation of the activation process, and the equations that describe Köhler theory can be used without the need to parametrize them, as is necessary in bulk models (Hoffmann *et al.*, 2015). This also allows for a direct

representation of aerosols within the simulations, instead of making assumptions about the nature and availability of the cloud condensation nuclei (CCNs). Furthermore, another advantage of the LCM approach is the way it considers the coupling between particles and the environment, avoiding entirely the so-called supersaturation adjustment approach (Grabowski *et al.*, 2018). By simulating the behavior of these SDs, the SDM can provide detailed insights into the microphysical processes that govern cloud and precipitation formation, which can be useful for improving weather forecasts and detailed studies of atmospheric phenomena. Despite its strengths, however, the SDM also has some limitations, including its reliance on somehow simplified assumptions about droplet properties and interactions (Grabowski *et al.*, 2019; Morrison *et al.*, 2020). Also, there is ongoing debate about the convergence and homogeneity of the results from different implementations of the collision–coalescence process using the SDM, which appear to differ from model to model (Hill *et al.*, 2023).

In this article, we will provide an overview of the current implementation of the SDM, including its collision–coalescence module. Then we will discuss the role of collision and coalescence on fog formation and examine the collisional activation process in a marine fog environment. The article is organized as follows: in Section 2, the modeling tool used will be described, as well as the simulation set-up, initial conditions, and experiment design; in Section 3, we will present results from the simulations defined in Section 2 and discuss the role of collisions in marine fog formation and development; finally, in Section 4, some conclusions will be drawn from the results in Section 3, along with some recommendations for future work.

2 | MODEL DESCRIPTION AND SET-UP

The modeling tool used for this study is the National Center for Atmospheric Research Turbulence with Lagrangian Particles (NTLP) model (Richter *et al.*, 2021; Sweet *et al.*, 2018), which solves the incompressible Navier–Stokes equations under the Boussinesq approximation via a third-order Runge–Kutta scheme (Spalart *et al.*, 1991). A full description of the NTLP formulation and parameters can be found in Helgans and Richter (2016) and Richter *et al.* (2021), but a brief overview and certain relevant details are provided here.

The particle module of NTLP is based on individual droplet physics (Macmillan *et al.*, 2022; Richter *et al.*, 2021). In line with the work of Shima *et al.* (2009), the particles represented by each SD share the same

attributes, such as position \mathbf{x}_p^i , radius r_p^i , temperature T_p^i , velocity \mathbf{v}_p^i , solute mass m_s^i , and hygroscopicity κ^i , whereas each SD stands for a ξ^i number of real particles (multiplicity). At each time step, the NTLF code solves the Lagrangian equations governing momentum, mass, and energy conservation for each of the i th SDs and calculates their coupling with the surrounding fluid. Details about the SDM formulation and numerical implementation into NTLF can be found in Richter *et al.* (2021).

2.1 | Particle hygroscopicity

Included in the formulation of NTLF are the full Köhler equations (Köhler, 1936; Pruppacher & Klett, 2010), which take into account both the solute and curvature terms with their full complexity, by means of their inclusion in the calculation of specific humidity at the droplet surface (Richter *et al.* (2021), their eq. 9). For more details about the formulation of the evolution of the dispersed phase (particles) of NTLF, please refer to Richter *et al.* (2021); Helgans and Richter (2016) and Sweet *et al.* (2018). Within this formulation, hygroscopicity is represented by means of the κ -Köhler theory (Petters & Kreidenweis, 2007), which makes use of a single parameter κ that is included in the particle growth equation in a way that it could be determined from experiments, depending on the relationship between the dry and wet diameters (Petters & Kreidenweis, 2007). This simplified parameter κ is very useful; but rather than define it as bulk, effective parameter, we link it directly to the individual solute terms in the Köhler equations that are being solved within NTLF:

$$\kappa = \frac{\nu\Phi\rho_s M_w}{\rho_w M_s}, \quad (1)$$

where ν is the total number of ions per dissociating molecule, Φ stands for the osmotic coefficient, ρ_s and ρ_w represent the densities of the solute and water respectively, and M_s and M_w indicate the molecular weight of the solute and water respectively. This formulation has the advantage of being directly related to known activities that make up the solute. While the hygroscopicity values calculated from Equation (1) are not the exactly the same as those from Petters and Kreidenweis (2007), the differences are considered negligible in comparison with the advantages it offers, as shown in Figure 1.

When considering collision-coalescence, the mixing of hygroscopicity must be taken into account. This mixing process is represented by Petters and Kreidenweis (2007) as a mixing rule based on the volume fractions of the

components of the interaction:

$$\kappa = \sum_i \varepsilon_i \kappa_i, \quad (2)$$

$$\varepsilon_i = \frac{V_{s_i}}{V_s}, \quad (3)$$

where ε_i is the volumetric fraction defined as the ratio of the solute volume of each colliding particle V_{s_i} and the total solute volume V_s . However, to make use of the previous volumetric mixing rule, this would require tracking the individual densities of each solute within each SD, which is not practical from a numerical point of view. Thus, the mixing rule was replaced with a more convenient mass-based formulation. This eliminates the need of tracking the solute densities during the entire simulation, making use of it only for defining the initial state of the SDs and then only tracking the solute mass of each particle. The fraction included in the model is then

$$\varepsilon_i = \frac{m_{s_i}}{m_s}, \quad (4)$$

where m_{s_i} and m_s are the individual and total solute masses respectively. The deviations from the original volume-based formulation of Petters and Kreidenweis (2007) are very small when compared with the mass-based formulation, as shown in Figure 1.

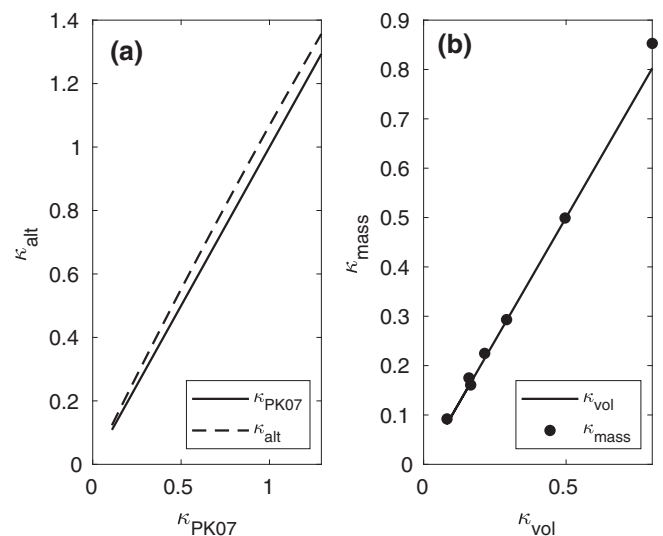


FIGURE 1 Hygroscopicity representation in the National Center for Atmospheric Research Turbulence with Lagrangian Particles model. (a) Comparison between hygroscopicity factor values following the original definition of Petters and Kreidenweis (2007) (κ_{PK07}) and its alternative definition implemented in the model (κ_{alt}). (b) Comparison between hygroscopicity factor values following the original volumetric mixing rule (κ_{vol}) and the mass-based mixing rule included in the model (κ_{mass}).

2.2 | Treatment of collision–coalescence and collisional activation

Following the framework of Shima *et al.* (2009), collision and coalescence are represented using a probabilistic algorithm. This is done by modifying the droplet radius r_p^i , solute mass m_p^i , hygroscopicity κ^i , and multiplicity ξ^i of both the collector and collected SDs, complying with the rules of mass conservation (Richter *et al.*, 2021). Particles within a certain region—Shima *et al.* (2009) chose the Eulerian grid cell, whereas we define a volume V independent of the large-eddy simulation (LES) grid—are subjected to a probability of collision as follows:

$$P_{jk} = E(r_p^j, r_p^k) \pi (r_p^j + r_p^k)^2 |\mathbf{v}_p^j - \mathbf{v}_p^k| \frac{\Delta t}{V}, \quad (5)$$

where j and k refer to the two interacting Lagrangian particles, and $E(r_p^j, r_p^k)$ refers to a collision efficiency. Note that by using the full velocity differences in Equation (5) we include potential effects of resolved turbulence in addition to differential settling (Richter *et al.*, 2021).

Although this formulation might increase the collision probability of particles, this is considered acceptable, since one of the effects of turbulence on the collision–coalescence process is that it modifies the relative velocity between the colliding droplets and changes the flow fields around the particles, therefore modifying the collision efficiency (Pinsky *et al.*, 2001; Seifert *et al.*, 2010). Indeed, when taking turbulence into account, the velocities of the drop approach are not equal to the difference in drop gravity velocities, and velocities are greater than in the pure gravity case (Seifert *et al.*, 2010). Thus, the collision efficiencies in a turbulent flow are usually greater than in calm air, and this effect is most pronounced in the case of small droplets, where the increase in collision efficiency is on average a factor of 2 and can increase up to a factor of 5 (Seifert *et al.*, 2010; Wang & Grabowski, 2009).

To obtain a more realistic representation of particles' collisions, a modified version of the collection efficiencies of Hall (1980) was used (Bott, 1998). This version utilizes data taken from Davis (1972) and Jonas (1972) for small particles, whereas for larger drops the dataset of Hall (1980) is used.

The understanding of unactivated particles (aerosols) and the processes that lead to their activation is dependent on the aerosols' physical, chemical, and dynamical properties. In NTLF, activation is calculated on a per-droplet basis by means of Köhler theory (Köhler, 1936), in which the local supersaturation plays a central role. Once exposed for a sufficiently long time to supersaturations exceeding the particles' critical supersaturation, a particle can

activate when it exceeds its critical radius r_c (Pruppacher & Klett, 2010). Owing to their small size, small aerosols become activated very quickly once the critical supersaturation value is reached, but for larger aerosols r_c becomes so large that activation by water vapor diffusion alone would take exceedingly long times, if it takes place at all. Recently, Hoffmann (2017) tested the limits of Köhler theory by exploring the role of collision–coalescence of aerosols on droplet activation through what he called “collisional activation”.

Following the methodology set forth by Hoffmann (2017), and in the framework of NTLF, we consider an aerosol particle activated once it reaches a certain size threshold corresponding to its critical radius r_c . As r_c is determined by calculating the maximum of the Köhler curve for each SD at each time step, the local supersaturation requirement is automatically fulfilled when diffusional activation is the dominant mechanism.

By selecting this approach, we acknowledge the existence of large CCNs that, by their size, behave as cloud/fog droplets. Such aerosols have a non-negligible collision rate and grow by diffusion in low supersaturation environments, despite not being formally activated, and have been reported in the literature (Dziekan *et al.*, 2021; Jensen & Nugent, 2017; Richter *et al.*, 2021). Although in order to better understand the behavior of such giant CCN particles an approach to classify water substance by means of a fixed size threshold is simpler and more appealing, we have chosen not to use it under the framework of this study, since it would make more difficult the understanding of how collision–coalescence affects fog formation and development at the activation stage. Using the critical radius approach provides a straightforward way to analyze the topic. An example of the applicability of the threshold approach can be found in Schwenkel and Maronga (2020). In their study, all particles larger than $1 \mu\text{m}$ were counted as fog droplets for comparison purposes with a bulk model, which is incapable of the level of detail provided by LCMs (Grabowski *et al.*, 2019), as well as to avoid the calculation of the critical radius at each time step for every SD, even though they acknowledge that those results probably include some swollen and not activated aerosols.

Fig. 3 of Hoffmann (2017) summarizes the different paths that lead to activation. To discern which process is dominating the activation of every particle during the simulations, the mass gain Δm of every particle must be tracked and attributed to its source: diffusional growth Δm_{diff} or accumulation of liquid water due to collection Δm_{coll} . If $\Delta m_{\text{diff}} > \Delta m_{\text{coll}}$ then the activation is classified as diffusional, whereas it is classified as collectional otherwise. This classification procedure is performed in the current model simulations following the numerical

algorithm and requirements provided in Hoffmann (2017). From collisional activation theory, we can elucidate two possible effects of collisions on aerosol activation. If an aerosol activates ($r > r_c$) and $\Delta m_{\text{coll}} > \Delta m_{\text{diff}}$, a direct collisional activation occurs. However, if, after a coalescence event, r remains lower than r_c then the aerosol is still inactivated, but it has gained mass (grown) from that collision, effectively accelerating its own activation, even if it activates by diffusion afterwards ($\Delta m_{\text{diff}} > \Delta m_{\text{coll}}$ at the time of activation).

2.3 | Numerical set-up, initial conditions, and experiment design

The simulation domain is identical to that of Wainwright *et al.* (2021) and Richter *et al.* (2021). It extends 128 m horizontally (x and y directions) and 80 m in the vertical z direction. This is smaller than conventional boundary-layer studies, but it is deemed sufficient for a shallow fog layer that forms in stable conditions Richter *et al.* (2021). Horizontally, $[N_x, N_y] = [128, 128]$ nodes are distributed equidistantly, resulting in a spatial resolution of $[\Delta x, \Delta y] = [1 \text{ m}, 1 \text{ m}]$. In the vertical direction, the same number of nodes ($N_z = 128$) is stretched to obtain a higher resolution at the lower levels where the fog layer is located, and less resolution near the top of the domain. This makes the vertical resolution vary over a range from $\Delta z = 0.1 \text{ m}$ at the bottom to nearly $\Delta z \approx 3 \text{ m}$ at the domain top.

As in Wainwright *et al.* (2021) and Richter *et al.* (2021), the simulation represents a case of advection fog where a parcel of saturated, warm air “moves” over a lower sea-surface temperature (SST). In practice, this is achieved by letting the model spin-up for 1 hr while in thermal equilibrium with water surface and then dropping the SST by 2 K, thereby mimicking the process of a saturated air mass in equilibrium with the lower surface abruptly being transported over cooler waters (Richter *et al.*, 2021; Wainwright *et al.*, 2021).

The SST is initially set to 284 K and at 1 hr is dropped to 282 K. The flow is forced with a constant geostrophic wind velocity with components $U_g = 4 \text{ m}\cdot\text{s}^{-1}$ and $V_g = 0$. The same initial thermodynamic profile from Richter *et al.* (2021) is used, which is based on conditions encountered on the C-FOG campaign (Fernando *et al.*, 2021): slightly stable, saturated stratification near the surface capped with a shallow inversion layer. The initial vertical profiles of potential temperature and water vapor mixing ratio can be seen in fig. 1a of Richter *et al.* (2021).

As for boundary conditions, periodicity is enforced in the horizontal direction. At the upper boundary, a no-flux condition is applied for momentum, energy, and water vapor, whereas Monin–Obukhov similarity theory is

employed at the lower surface to calculate surface fluxes with a roughness length of $z_0 = 3.2 \times 10^{-5} \text{ m}$. A uniform SST is used, as described earlier herein, and q_v is fixed based on the SST such that the surface is always at 100% saturation (Richter *et al.*, 2021).

Following Richter *et al.* (2021), SDs are distributed randomly throughout the entire domain at the beginning of the simulation. The initial SDs begin unactivated, and they only activate by means of diffusion or collisions as the simulation evolves. To initialize the Lagrangian particles, we use a characterization of the dry ASD, with data from a fog event encountered during the C-FOG cruise (Fernando *et al.*, 2021). The aerosol diameter-based (d_a) distribution is clearly bimodal in nature, with maxima around $d_a \approx 0.1 \mu\text{m}$ and $d_a \approx 1 \mu\text{m}$. We consider these peaks to be the accumulation and coarse aerosol modes respectively and model this dry ASD ($P_{a,\text{init}}$) as the sum of two lognormal probability density functions (PDFs) (Richter *et al.*, 2021) as follows:

$$P_{a,\text{init}}(d_a) = \frac{1}{1+\gamma} \frac{1}{\sigma_a d_a \sqrt{2\pi}} \exp\left\{-\frac{[\ln(d_a) - \mu_a]^2}{2\sigma_a^2}\right\} + \frac{\gamma}{1+\gamma} \frac{1}{\sigma_c d_a \sqrt{2\pi}} \exp\left\{-\frac{[\ln(d_a) - \mu_c]^2}{2\sigma_c^2}\right\}. \quad (6)$$

In Equation (6), the parameters $\mu_a = -1.95$, $\sigma_a = 0.5$ and $\mu_c = 0$, $\sigma_c = 0.45$ effectively determine the location and width of the accumulation- and coarse-mode peaks respectively, and the parameter $\gamma = 0.02$ is a balancing multiplicative factor that reduces the probability of coarse-mode aerosols relative to that of the accumulation mode (Richter *et al.*, 2021). These parameters were obtained from fitting Equation (6) to C-FOG aerosol data (see fig. 1b of Richter *et al.* (2021)).

The initialization procedure makes use of the factor γ to probabilistically determine whether the SD generated will be from the accumulation- or coarse-mode regime; then, once this is decided, the dry diameter d_a is drawn from the lognormal distribution associated with that mode. From this, the solute mass is calculated, assuming a solute density of $\rho_s = 2000 \text{ kg}\cdot\text{m}^{-3}$. The initial SD temperature T_p^i is set to the ambient temperature. For more details about the SD initialization procedure, please refer to Richter *et al.* (2021).

As we intend to simulate a fog layer in a marine environment, the coarse mode is often composed primarily of marine salt, whereas the accumulation mode is often anthropogenic in origin (Chisholm *et al.*, 2021; Zhang *et al.*, 2014). This is captured in the simulations in a simple way by setting all hygroscopicities from the accumulation mode to $\kappa^i = 0.6$ (ammonium sulfate) and all hygroscopicities from the coarse mode to $\kappa^i = 1.2$

TABLE 1 Summary of the experiment design.

Experiment	Aerosol concentration (cm ⁻³)	Condensation	Collision-coalescence
Exp. 1	100	Yes	No
Exp. 2	800	Yes	No
Exp. 3	2000	Yes	No
Exp. 4	100	Yes	Yes
Exp. 5	800	Yes	Yes
Exp. 6	2000	Yes	Yes

(sea salt), reflecting rough estimates of continental and marine values respectively (Petters & Kreidenweis, 2007).

According to Shima *et al.* (2009), a good rule of thumb for an adequate number of SDs for representing the full ASD/DSD at each of the LES grid nodes should be between 50 and 100 SDs per Eulerian grid cell. Though prior research has compared collision-coalescence algorithms in box model simulations (Dziekan & Pawlowska, 2017; Unterstrasser *et al.*, 2017), such comparisons have yet to be extended to one-dimensional cloud simulations (Hill *et al.*, 2023). In multidimensional models, collection/aggregation might be further influenced by the movement of SDs due to sedimentation or flow dynamics. Hence, it is not clear which findings of their evaluation efforts are the most relevant aspects that control the performance of collection/aggregation algorithms in more complex LCM simulations (Unterstrasser *et al.*, 2017). Thus, owing to the very high spatial resolution of our LES grid, as well as the large computational expense of using $\mathcal{O}(100)$ SDs (not feasible with our current computational resources), we chose to use 64 SDs per grid cell, giving a total of $N_p = 13,4217,728$ Lagrangian particles in the entire domain.

Regarding boundary conditions for the droplet/aerosols, a no-flux condition is imposed at the upper boundary. At the bottom of the domain, droplets that hit the water surface are removed from the simulation and a new SD is immediately introduced randomly in the domain according to the same procedure for initialization. This maintains a constant number of SDs in the simulation throughout the entire duration so that certain statistics are quasi-steady-state (Richter *et al.*, 2021).

To isolate the effects of collision-coalescence on marine fog formation, we have conducted two sets of experiments. In the first set, the particles are only allowed to grow by condensation, neglecting collision-coalescence entirely. In the second set, collision-coalescence is turned on alongside diffusional growth. In addition, each experiment is performed across a variety of ambient aerosol loads that includes pristine, regular, and aerosol-laden environments (Table 1). In our simulations, the bulk

particle number concentration effectively sets the initial multiplicity ξ^i for each superdroplet, following Shima *et al.* (2009).

3 | RESULTS

In the previous section we suggested that collision and coalescence of aerosol particles can contribute to the particles' mass gain required for activation. In this section, we will illustrate the effect that this process has on fog formation. After running the experiments previously defined, a fog layer less than 30 m thick starts to form after 5 hr into the simulations. As shown in Figure 2, the difference in fog onset time due to collisions is negligible (less than 20 min). However, the simulations with condensation only show more liquid water mass and lower particle number concentration than when taking collisions into account, inside the fog layer. This means that, within the framework of these simulations, collisions are responsible for certain changes in the microphysical characteristics of marine fog, but not necessarily in the bulk behavior of the fog layer itself.

As shown in Figure 3, there is a marked difference between the resulting fog DSDs with and without collisions. The experiments with collision-coalescence exhibit a larger concentration of small droplets, particularly at 6 hr. This behavior, however, is opposite to what one might expect in clouds, especially preceding precipitation. Clearly, although collisions do not affect onset time of fog, they do affect the shape and structure of the DSD at the formation and development stages of the simulated fog layer.

Figure 4a shows the average radius of the activated droplets inside the fog layer for Expt. 2 and Expt. 5. Consistent with Figure 3, particle collisions continuously lead to smaller mean droplet sizes after the fog layer starts to form, with larger mean radii in the case that considers diffusional growth only. In addition to this, Figure 4b shows a larger number of activated particles in the experiments that include collisions, which indicates that collisional activations, or some other indirect effect due to the collisions, is taking place.

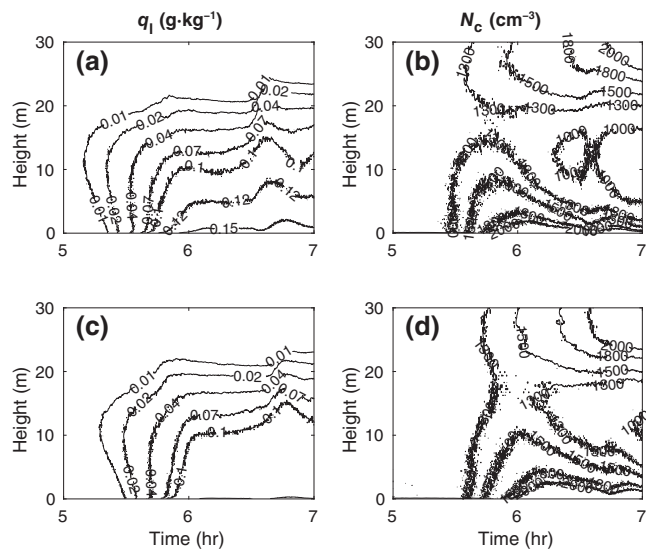


FIGURE 2 Time–height plots of the horizontally averaged (a,c) liquid water mixing ratio q_l and (b,d) particle number concentration N_c . For the sake of clarity, only Exp. 2 (condensation only; a, b) and Exp. 5 (condensation and collisions; c, d) are shown, due to similar behavior with the rest of the cases.

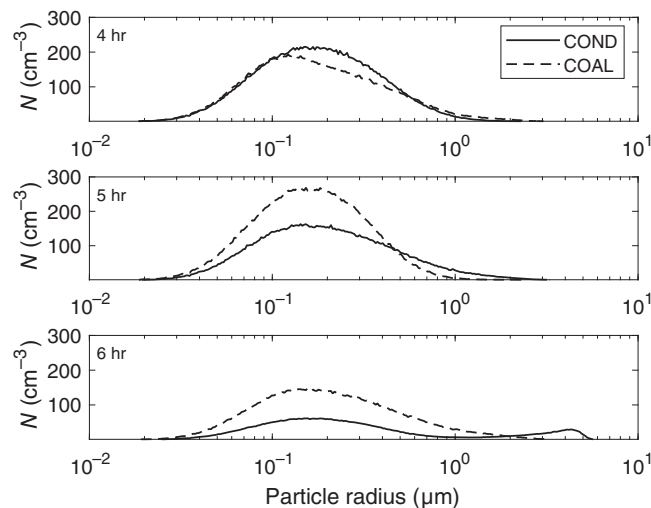


FIGURE 3 Droplet size distribution at 4 hr (top panel), 5 hr (middle panel), and 6 hr (bottom panel) into the simulations. For the sake of clarity, only Exp. 2 (labeled as COND, solid black line) and Exp. 5 (labeled as COAL, dashed black line) are shown, owing to similar behavior with the rest of the cases.

To better discern the possible causes of this behavior, Figure 5 shows multiple vertical profiles associated with activation differences between the cases with and without collisions. Figure 5a shows the maximum diffusion radius (MDR), which is the largest critical radius of an aerosol activated exclusively by diffusion at a certain height. Figure 5b,c plots the supersaturation and the collectional activation rate respectively. The collectional

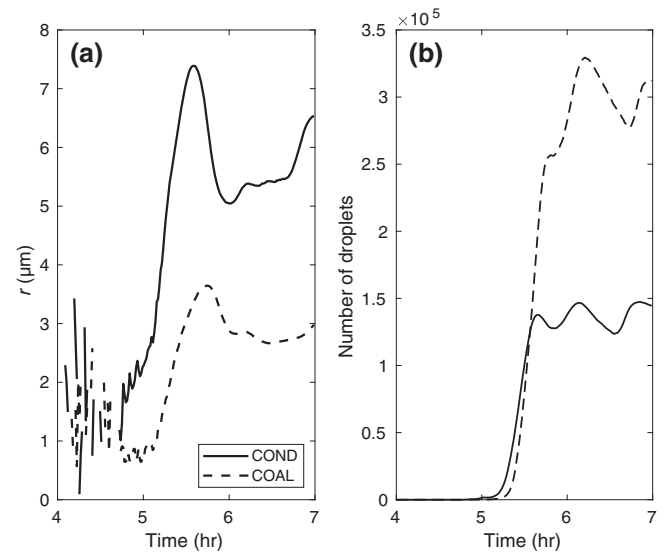


FIGURE 4 Side-by-side panels of (a) average radius of activated droplets inside the fog layer and (b) number of activated particles per time step. For the sake of clarity, only Exp. 2 (labeled as COND, solid black line) and Exp. 5 (labeled as COAL, dashed black line) are shown, owing to similar behavior with the rest of the cases.

activation rate is defined as the number of aerosols activated by collection per unit of volume and time. Lastly, Figure 5d shows the corresponding diffusional activation rate (DAR). Only data from the last simulated hour is considered. As MDR, supersaturation, and diffusional activation rate profiles from Exp. 1, 2, and 3 look very similar to those from Exp. 4, 5, and 6 respectively, only data from the last three are shown.

The vertical location of the MDR coincides with the higher values of supersaturation, reaching the maximum values around the center of the fog layer (approximately 15m). In addition to this, supersaturation and MDR are generally smaller with higher particle concentration, with the smallest values observed in the polluted simulation. This might be due to the larger number of aerosols absorbing water vapour. Collectional activation rate (Figure 5c) decreases with height, with a more pronounced slope in the aerosol-laden simulations (2000 cm^{-3} , Exp. 6). Furthermore, the shape of the diffusional activation rate (Figure 5d) appears uniform throughout the fog layer, rapidly decreasing with height at the top due to exposure to negative supersaturations.

Another observation that can be made from the activation rates in Figure 5c,d is that the contribution of collectional activation to the number of activated aerosols is significantly smaller than the contribution of diffusional activation, with a difference of four orders of magnitude in some cases. Figure 6 confirms that only a very small percentage of activations are caused by the collision–coalescence process (around 0.00103% on

FIGURE 5 Vertical profiles of (a) maximum diffusion radius (MDR), (b) supersaturation (SS), (c) collectional activation rates (CAR), and (d) diffusional activation rates (DAR) for pristine (100 cm^{-3} , solid black line), regular (800 cm^{-3} , dashed black line), and polluted ($2,000\text{ cm}^{-3}$, dash-dot black line) environments. The data are taken from the last hour of the simulations.

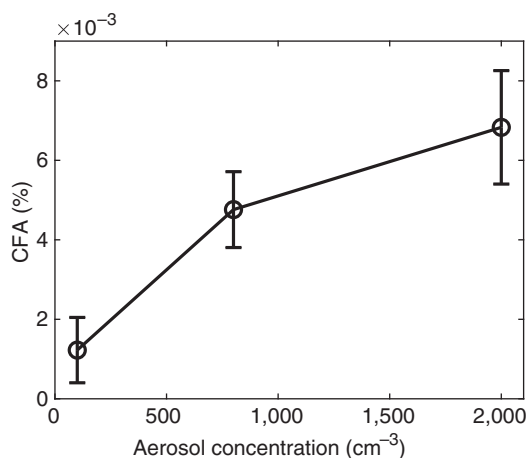
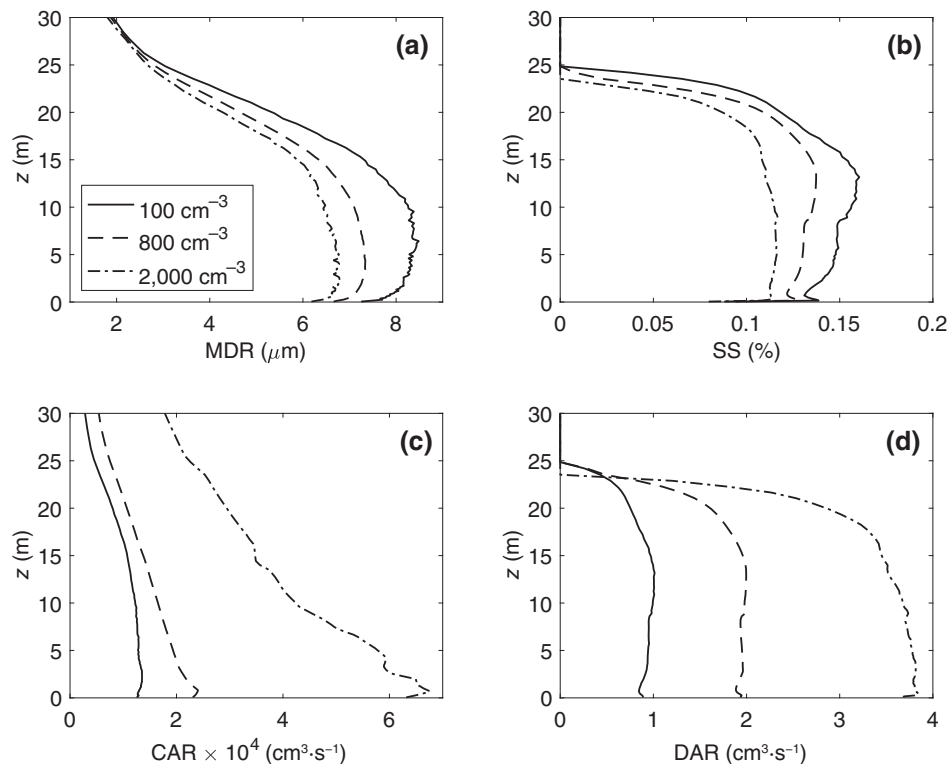


FIGURE 6 Collectional fraction of activations (CFA). The error bars indicate the standard deviation for each experiment. The data are taken from the last hour of the simulations.

average). This collectional fraction of activations (CFA, fraction of activations that are attributed to collisions) increases in more polluted environments, which can be attributed simply to the fact that the larger number of aerosols increases the likelihood of activation. The CFA values obtained here are smaller than (but within the same order of magnitude as) the findings of Hoffmann (2017), who found the CFA to be around 0.008% in trade wind cumuli. The differences are because the particles found inside a fog layer are generally smaller than those in stratocumulus clouds, and hence there is a decrease in the number of collision events that lead to activation.

Figure 7 shows the size-dependent collectional and diffusional fraction of activations. This is similar to the aforementioned CFA, in that they represent the percentage of activations that can be attributed to one process or another, but now as a function of dry aerosol radius. Unsurprisingly, diffusional activation is the main driver for the activation of small aerosols (dry radius below $0.3\text{ }\mu\text{m}$). The curves that describe diffusional activation shift toward the right (larger radius values) as the aerosol number concentration is reduced, owing to the higher supersaturation (see Figure 5b) in more pristine conditions. This results in a more significant overlap with the collectional activation fraction curves. For aerosols larger than $0.3\text{ }\mu\text{m}$, activation through collection gains importance, since the particles are large enough to provoke collisions. In the range between $0.3\text{ }\mu\text{m}$ and $0.6\text{ }\mu\text{m}$, both the diffusional and collectional paths contribute equally to the overall activation process. Finally, for aerosols with dry radius larger than $0.6\text{ }\mu\text{m}$, collectional activation becomes the dominant process for the creation of activated droplets inside the simulated fog layer, indicating a significant effect of collectional activation on this part of the aerosol spectrum. This threshold is dependent on the aerosol concentration, with collisional activation gaining importance at increasingly smaller radii as the aerosol concentration increases. This could be because of the smaller sizes that can be reached by condensation alone, due to less available water vapor, which slows down the diffusional activation in favor of the collectional path. Also, since the smaller particles are much more numerous than the larger ones,

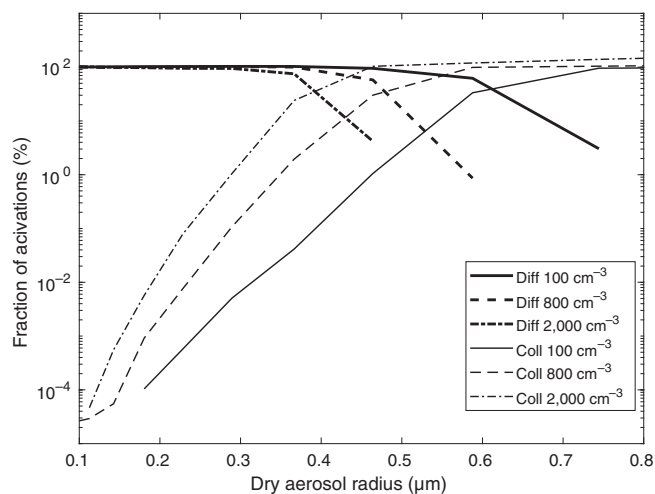


FIGURE 7 Comparison of collectional (thin lines) and diffusional (thick lines) fraction of activations for pristine (100 cm^{-3} , solid black line), regular (800 cm^{-3} , dashed black line), and polluted ($2,000\text{ cm}^{-3}$, dash-dot black line) environments. The data are taken from the last hour of the simulations.

they represent a larger proportion of the aerosols activated by collectional activation. Larger aerosols outside of the range of the figure do not activate at all because their critical supersaturations/radii are too large to be reached by either process. This direct effect of collisional activation enables the activation of larger aerosols, which would otherwise not be able to become droplets by diffusion alone. This partially explains the larger number of activated droplets in the collision-permitting simulations (see Figure 4b), but not the smaller sizes in relation to the condensation runs.

So far we have explored collision-coalescence as a path for aerosol activations inside a fog layer. However, a question remains regarding the larger number of small particles in the coalescence simulations (cf. Figure 3), since it cannot be explained by the number of collisional activations alone. To this end, Figure 8 shows the fraction of particles that were activated (either as a result of diffusion or collisions) with at least some mass contributions from coalescence (i.e., each activated droplet is interrogated as to whether it had ever participated in a collision-coalescence event prior to activation). As defined in Section 2.2, only particles activated with a collisional mass contribution higher than 50% of the aerosol's mass content at the moment of activation are classified as collisional. But particles with smaller mass contributions from collisions, and not classified as collisionally activated, also acquire a significant fraction of their size from coalescence. In fact, collisions represent between 2% and 30% of the total mass gain that counts toward activation, across all activated droplets.

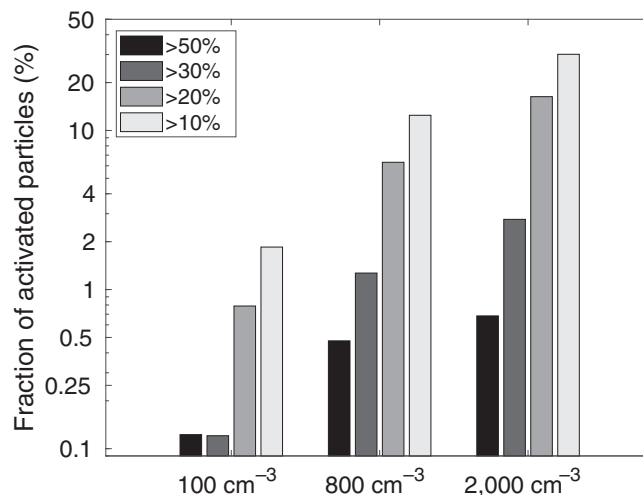
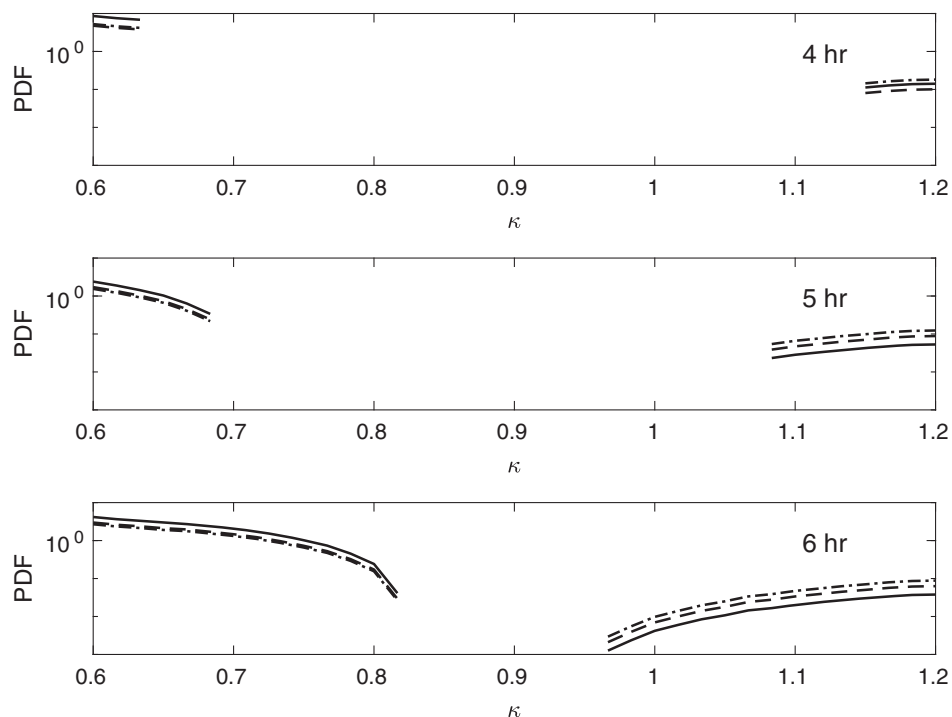


FIGURE 8 Fraction of droplets that were activated with mass contributions from collision-coalescence for pristine (100 cm^{-3}), regular (800 cm^{-3}), and polluted ($2,000\text{ cm}^{-3}$) environments. The ordinate (y) axis shows the percentage fraction of particles that activate, and the legend shows the percentage fraction of mass that contributes to particle growth due to collision-coalescence only. The data are taken from the last hour of the simulations.

This is particularly true for higher aerosol concentrations (polluted case, 2000 cm^{-3}), where one-fifth of the activated particles gained 20% of their mass via collisions, and this number increases to almost two-fifths if we consider a contribution of 10% of the total mass. For a moderate aerosol load (800 cm^{-3}), this contribution is between 10% and 20%. For pristine environments (100 cm^{-3}) the contribution is less than 2%, and thus negligible. This is an indication that collisions not only can cause the activation of aerosols, but can also accelerate their activation via water vapor diffusion, thanks to the mass gain from the collisions themselves. This indirect effect of collision and coalescence of particles facilitates the activation of a larger number of small aerosols, partially explaining the enhanced small droplet production in the coalescence simulations appreciated in the DSD (Figures 3 and 5b).

However, the question remains as to how this relatively small mass contribution (nominally less than 10% of the mass) from collisions can cause such an acceleration of the diffusional activation rates. In this case, the answer lies in the way the collision-coalescence algorithm is represented within the model. When two particles collide (either aerosols, droplets, or a combination of both), their hygroscopicity changes following the mixing rule explained in Equation (2). In this regard, Figure 9 shows the time evolution of the hygroscopicity parameter κ PDF. At 4 hr into the simulations, κ values have barely changed from the initial conditions (which consists of delta functions at $\kappa = 0.6$ and $\kappa = 1.2$), because the background particles are

FIGURE 9 Probability density function (PDF) of the hygroscopicity parameter κ at 4 hr (top panel), 5 hr (middle panel), and 6 h (bottom panel) into the simulations. The plots are for pristine (100 cm^{-3} , solid black line), regular (800 cm^{-3} , dashed black line), and polluted ($2,000 \text{ cm}^{-3}$, dash-dot black line) environments.



not big enough to cause sufficient collisions to alter this significantly. However, once the fog layer starts to form (positive supersaturations are reached) and the aerosols start to grow by diffusion, the shape of the hygroscopicity PDF changes significantly, shifting toward the center. As the fog layer is developing, collisions cause a homogenizing effect on the particles' hygroscopicities. Going deeper into this effect, Figure 9 shows that, after 6 hr into the simulations, the hygroscopicity of the coarse-mode aerosols decreases to around 0.97. This is because their size allows them collect a large number of lower hygroscopicity particles, thereby decreasing their diffusional growth rate. This results in the inhibition (to some degree) of the activation of large particles via water vapor diffusion, which explains the absence of a second mode in the coalescence simulation shown in Figure 3.

The opposite effect is observed in the aerosols originally located in the accumulation mode (Figure 9). Right after fog starts to form, their size is too small to undergo many collisions; thus, their hygroscopicity change is slow. Once diffusional growth kicks in, accumulation-mode aerosols increase their hygroscopicity to approximately 0.81 (as shown in Figure 9). This increase in κ then enhances their future activation tendency, and hence the increased activation of small-size droplets (between $0.1 \mu\text{m}$ and $1 \mu\text{m}$) observed in Figures 3 and 5b. It is noteworthy that the increase in hygroscopicity for accumulation-mode aerosols is similar in magnitude to the decrease in the coarse-mode particles, despite the former lower collection efficiencies associated with their small size. A possible explanation for this lies on their sheer

quantity: as accumulation-mode aerosols are much more numerous than the coarse mode ones, their number helps offset the lower collision probability.

This indirect process of modifying the hygroscopicity cannot take place in the simulations that neglect collision-coalescence (Exp. 1, 2, and 3 in Table 1). Thus, the coarse-mode aerosols (with high hygroscopicity) grow unhindered, as a result of the local ambient supersaturation, developing a second mode in the DSD purely by water vapor diffusion onto the surface of the particles. The absence of collisions also delays the growth of the accumulation-mode aerosols, via the fixed lower value of the hygroscopicity parameter, tying them to slow condensational growth for the entirety of the simulations.

4 | CONCLUSIONS

The role of collision and coalescence on marine fog formation has been discussed by means of LESs coupled with a Lagrangian cloud model (NTLP), based on events observed during the C-FOG campaign. Although the effect of collisions on fog onset time is negligible, it has been found that it changes the structure of the DSD before and after the formation stage. The simulations showed that, when collision-coalescence is taken into account, the simulations produce a large number of smaller droplets inside a fog layer.

Based on the recently developed "collisional activation" theory (Hoffmann, 2017), it was found that inactivated aerosols inside a marine fog layer can be activated by

the collection of aerosol particles. Our simulations showed that the collectional activation rate decreases with height inside the fog layer, whereas the slope and the height from which collectional activation starts increase with aerosol concentration, this effect being more pronounced in polluted marine environments. Also, though the actual fraction of droplets activated by collisions is very small, more aerosol concentration leads to an enhanced CFA. This path to activation also enables the activation of larger aerosols previously considered to be impossible to activate due to their excessive critical radius. This partially explains the larger number of activated droplets in the collision-permitting simulations, but not the smaller sizes in relation to the condensation runs. Although diffusion dominates the growth of small aerosols, collisional activation gains some importance for aerosols with dry radius larger than $0.3 \mu\text{m}$ and becomes the main driver for activation for aerosols larger than $0.6 \mu\text{m}$. However, although activation via collisions is possible, diffusional growth is still necessary to create aerosols large enough to be able to collide.

In addition to the direct effect of the collisional activation, it was found that its indirect effects are even more important in fog. First, collisions have proved to be an important source of mass to the aerosols, contributing between 2% and 30% of the total mass gain toward activation, allowing them to grow faster toward their critical radii and shortening the time needed to activate by diffusion. This partially explains the enhanced small droplet production in the coalescence simulations appreciated in the DSD. Second, but no less important, is how collisions continually homogenize the aerosol hygroscopicity across the assumed low-hygroscopicity accumulation-mode particles and the high-hygroscopicity coarse-mode particles. By increasing the hygroscopicity (via collisions) of the aerosols originally located in the accumulation mode, this also facilitates their future activation by condensation. As these aerosols are much more numerous than the coarse-mode ones, their change in hygroscopicity makes their future activation by diffusion easier. To the best of our knowledge, no previous numerical studies have taken this into account.

One of the most interesting interpretations of this study, besides demonstrating collision-coalescence as a path for facilitating activation and a source of droplets inside a marine fog layer, is the fact that aerosol particles within a certain range are able to grow by condensation, collide, coalesce, and sediment, exhibiting effectively the behavior of activated droplets—despite not being technically activated. This raises the question of the importance of these oft-neglected, droplet-like particles in the modeling of marine fog. Similar questions are being addressed about so-called giant CCN particles which, despite their

low number, contribute to precipitation formation in marine environments (Jensen & Lee, 2008; Jensen & Nugent, 2017).

Furthermore, though the total amount of liquid water content and the spatial distribution of the two main bulk variables (q_l and N_c) do not vary much, the microphysical structure of the DSD, droplet number, and concentration are certainly influenced by the two collision indirect effects summarized herein. Besides the already discussed consequences on the microphysical properties of fog, this could have strong implications on visibility, which is known to be dependent on particle concentration. In addition, the size and number of particles effectively determine its radiative contribution, which is a known crucial factor throughout the fog life cycle. Hence, collisions play a secondary but important role in marine fog development and should not be ignored in future numerical studies of this phenomenon.

Before concluding, we would like to highlight some of the differences between the results presented here and those in clouds (Hoffmann, 2017). First, the numerical experiments were performed for the study of a totally different process, which is marine fog formation and development. Our findings show that the collisional fraction of activations in fog is eight times lower than in trade wind cumuli. Second, the practical threshold for collisional activation to have a relevant role is higher in marine fog, three times higher than its value in trade wind cumuli ($0.1 \mu\text{m}$). This is also the case for the size after which aerosols can exclusively be activated by collisions. These differences can be attributed to the generally smaller particle sizes found inside fog, in contrast with those in clouds. Third, for clouds, it was found that collisional activation is not particularly important for determining the number of cloud droplets. Though this is also true for our simulations of marine fog, particle collisions enable the possibility of occurrence of two important indirect effects that could possibly change the number of activated droplets and the shape of the DSD: aerosol mass contribution accelerates the activation process via diffusional growth, and the collisions' homogenizing effect on particle hygroscopicity somehow inhibits diffusional growth of coarse-mode particles, while shortening activation time of the smaller accumulation-mode aerosols.

Finally, we will enumerate the the potential sources of uncertainty in this study. First, the mathematical formulation of the collision-coalescence module of the model can greatly influence the results. For instance, the accuracy of the collection kernel of (Hall, 1980) is questionable for small particles, having been argued that it increases their collection probability. Even with the use of the modified Hall kernel (Bott, 1998), it remains a potential source of uncertainty. Moreover, the collection kernel might not

incorporate all processes relevant for collections among aerosols and droplets. The effects of turbulence on the collection rates, for example, is not directly taken into account. Although this is alleviated by the use of the full vector differences in the velocity of the particles, Equation (5), the actual role of turbulence on collisional activation remains unknown. Second, the chemical composition of the initial ASD is a somewhat crude approximation of real-life conditions. A better description of the chemical composition and hygroscopicity of the background ASD would be needed for a more precise assessment of the role of the varying hygroscopicity PDF in the activation process (Chisholm *et al.*, 2021). Third, the collection algorithm itself within the framework of the SDM might be an additional source of uncertainty. It is known that the SDM is a good benchmark for the process of diffusional growth of particles, but once collision-coalescence is considered, the results between the different Lagrangian cloud models vary greatly (Hill *et al.*, 2023). There are considerable efforts in the modeling community to tackle this problem, but a common framework for collisions is still in development.

ACKNOWLEDGEMENTS

We would like to thank the University of Notre Dame Center for Research Computing for providing, managing, and maintaining the computational resources without which this study would have been impossible. This research is funded by the Office of Naval Research, by means of the Office of Naval Research (grant number N00014-21-1-2296; N00014-18-1-2472).

CONFLICT OF INTEREST STATEMENT

The authors declare no conflict of interest.

DATA AVAILABILITY STATEMENT

Data available on request from the authors.

ORCID

Camilo F. Rodriguez-Geno  <https://orcid.org/0000-0002-6176-7577>

David H. Richter  <https://orcid.org/0000-0001-6389-0715>

REFERENCES

- Barros, A.P., Prat, O.P., Shrestha, P., Testik, F.Y. & Bliven, L.F. (2008) Revisiting Low and List (1982): Evaluation of raindrop collision parameterizations using laboratory observations and modeling. *Journal of the Atmospheric Sciences*, 65, 2983–2993. Available from: <https://journals.ametsoc.org/doi/10.1175/2008JAS2630.1>
- Berry, E.X. (1967) Cloud droplet growth by collection. *Journal of the Atmospheric Sciences*, 24, 688–701.
- Berry, E.X. & Reinhardt, R.L. (1974) An analysis of cloud drop growth by collection: Part I. Double distributions. *Journal of the Atmospheric Sciences*, 31, 1814–1824.
- Bott, A. (1998) Program for the solution of the stochastic coalescence equation: One-dimensional cloud microphysics. <https://doi.org/10.5281/zenodo.5660185>.
- Boutle, I., Angevine, W., Bao, J.-W., Bergot, T., Bhattacharya, R., Bott, A. et al. (2022) Demistify: a large-eddy simulation (LES) and single-column model (SCM) intercomparison of radiation fog. *Atmospheric Chemistry and Physics*, 22, 319–333. Available from: <https://acp.copernicus.org/articles/22/319/2022/>
- Chen, C., Zhang, M., Perrie, W., Chang, R., Gultepe, I., Fernando, H.J.S. et al. (2021) A case study: Evaluation of PAFOG one-D model with advection in simulations of fog/stratus from C-FOG experiment. *Journal of Geophysical Research: Atmospheres*, 126, e2021JD034812. Available from: <https://onlinelibrary.wiley.com/doi/full/10.1029/2021JD034812>
- Chisholm, N., Nagare, B., Wainwright, C., Creegan, E., Salehpoor, L., VandenBoer, T.C. et al. (2021) Characterizing atmospheric aerosols off the Atlantic Canadian coast during C-FOG. *Boundary-Layer Meteorology*, 181, 345–364. Available from: <https://doi.org/10.1007/s10546-021-00673-7>
- Clark, T.L. & Hall, W.D. (1983) A cloud physical parameterization method using movable basis functions: Stochastic coalescence parcel calculations. *Journal of the Atmospheric Sciences*, 40, 1709–1728.
- Davis, M.H. (1972) Collisions of small cloud droplets: Gas kinetic effects. *Journal of the Atmospheric Sciences*, 29, 911–915.
- Dimitrova, R., Sharma, A., Fernando, H.J.S., Gultepe, I., Danchofski, V., Wagh, S. et al. (2021) Simulations of coastal fog in the Canadian Atlantic with the weather research and forecasting model. *Boundary-Layer Meteorology*, 181, 443–472. Available from: <https://link.springer.com/article/10.1007/s10546-021-00662-w>
- Dziekan, P., Jensen, J.B., Grabowski, W.W. & Pawlowska, H. (2021) Impact of giant sea salt aerosol particles on precipitation in marine cumuli and stratocumuli: Lagrangian cloud model simulations. *Journal of the Atmospheric Sciences*, 78, 4127–4142. Available from: <https://journals.ametsoc.org/view/journals/atsc/78/12/JAS-D-21-0041.1.xml>
- Dziekan, P. & Pawlowska, H. (2017) Stochastic coalescence in Lagrangian cloud microphysics. *Atmospheric Chemistry and Physics*, 17, 13509–13520. Available from: <https://acp.copernicus.org/articles/17/13509/2017/>
- Fernando, H.J.S., Gultepe, I., Dorman, C., Pardyjak, E., Wang, Q., Hoch, S.W. et al. (2021) C-FOG: Life of coastal fog. *Bulletin of the American Meteorological Society*, 102, E244–E272. Available from: <https://journals.ametsoc.org/view/journals/bams/102/2/BAMS-D-19-0070.1.xml>
- Grabowski, W.W., Dziekan, P. & Pawlowska, H. (2018) Lagrangian condensation microphysics with Twomey CCN activation. *Geoscientific Model Development*, 11, 103–120. Available from: <https://gmd.copernicus.org/articles/11/103/2018/>
- Grabowski, W.W., Morrison, H., Shima, S.-I., Abade, G.C., Dziekan, P. & Pawlowska, H. (2019) Modeling of cloud microphysics: Can we do better? *Bulletin of the American Meteorological Society*, 100, 655–672. Available from: <https://journals.ametsoc.org/doi/10.1175/BAMS-D-18-0005.1>
- Gultepe, I., Heymsfield, A.J., Fernando, H.J.S., Pardyjak, E., Dorman, C.E., Wang, Q. et al. (2021) A review of coastal fog microphysics during C-FOG. *Boundary-Layer Meteorology*, 181, 227–265. Available from: <https://link.springer.com/10.1007/s10546-021-00659-5>

- Gultepe, I., Milbrandt, J.A. & Zhou, B. (2017) Marine fog: A review on microphysics and visibility prediction. In: Koraćin, D. & Dorman, C.E. (Eds.) *Marine fog: Challenges and Advancements in Observations, Modeling, and Forecasting*. Cham: Springer International Publishing, pp. 345–394. Available from: http://link.springer.com/10.1007/978-3-319-45229-6_7
- Gultepe, I., Tardif, R., Michaelides, S.C., Cermak, J., Bott, A., Bendix, J. et al. (2007) Fog research: A review of past achievements and future perspectives. *Pure and Applied Geophysics*, 164, 1121–1159. Available from: <http://link.springer.com/10.1007/s00024-007-0211-x>
- Hall, W.D. (1980) A detailed microphysical model within a two-dimensional dynamic framework: Model description and preliminary Results. *Journal of the Atmospheric Sciences*, 37, 2486–2507.
- Helgans, B. & Richter, D.H. (2016) Turbulent latent and sensible heat flux in the presence of evaporative droplets. *International Journal of Multiphase Flow*, 78, 1–11.
- Hill, A.A., Lebo, Z.J., Andrejczuk, M., Arabas, S., Dziekan, P., Field, P. et al. (2023) Toward a numerical benchmark for warm rain processes. *Journal of the Atmospheric Sciences*, 80, 1329–1359. Available from: <https://journals.ametsoc.org/view/journals/atsc/aop/JAS-D-21-0275.1/JAS-D-21-0275.1.xml>
- Hoffmann, F. (2017) On the limits of Köhler activation theory: How do collision and coalescence affect the activation of aerosols? *Atmospheric Chemistry and Physics*, 17, 8343–8356. Available from: <https://acp.copernicus.org/articles/17/8343/2017/>
- Hoffmann, F., Raasch, S. & Noh, Y. (2015) Entrainment of aerosols and their activation in a shallow cumulus cloud studied with a coupled LCM-LES approach. *Atmospheric Research*, 156, 43–57. Available from: <https://linkinghub.elsevier.com/retrieve/pii/S016980951400444X>
- Jensen, J.B. & Lee, S. (2008) Giant sea-salt aerosols and warm rain formation in marine stratocumulus. *Journal of the Atmospheric Sciences*, 65, 3678–3694. Available from: <https://journals.ametsoc.org/view/journals/atsc/65/12/2008jas2617.1.xml>
- Jensen, J.B. & Nugent, A.D. (2017) Condensational growth of drops formed on giant sea-salt aerosol particles. *Journal of the Atmospheric Sciences*, 74, 679–697. Available from: <https://journals.ametsoc.org/view/journals/atsc/74/3/jas-d-15-0370.1.xml>
- Jonas, P.R. (1972) The collision efficiency of small drops. *Quarterly Journal of the Royal Meteorological Society*, 98, 681–683. Available from: <https://onlinelibrary.wiley.com/doi/full/10.1002/qj.49709841717>
- Köhler, H. (1936) The nucleus in and the growth of hygroscopic droplets. *Transactions of the Faraday Society*, 32, 1152–1161. Available from: <https://pubs.rsc.org/en/content/articlepdf/1936/ft/ft9363201152>
- Koraćin, D., Dorman, C.E., Lewis, J.M., Hudson, J.G., Wilcox, E.M. & Torregrosa, A. (2014) Marine fog: A review. *Atmospheric Research*, 143, 142–175. Available from: <https://linkinghub.elsevier.com/retrieve/pii/S016980951300361X>
- Low, T.B. & List, R. (1982) Collision, coalescence and breakup of raindrops. Part I: Experimentally established coalescence efficiencies and fragment size distributions in breakup. *Journal of the Atmospheric Sciences*, 39, 1591–1606. Available from: [https://doi.org/10.1175/1520-0469\(1982\)039<1591:CCABOR>2.0.CO;2](https://doi.org/10.1175/1520-0469(1982)039<1591:CCABOR>2.0.CO;2)
- Macmillan, T., Shaw, R.A., Cantrell, W.H. & Richter, D.H. (2022) Direct numerical simulation of turbulence and microphysics in the Pi Chamber. *Physical Review Fluids*, 7, 020501. Available from: <https://journals.aps.org/prfluids/abstract/10.1103/PhysRevFluids.7.020501>
- Mazoyer, M., Lac, C., Thouron, O., Bergot, T., Masson, V. & Musson-Genon, L. (2017) Large eddy simulation of radiation fog: Impact of dynamics on the fog life cycle. *Atmospheric Chemistry and Physics*, 17, 13017–13035.
- Morrison, H., Lier-Walqui, M., Fridlind, A.M., Grabowski, W.W., Harrington, J.Y., Hoose, C. et al. (2020) Confronting the challenge of modeling cloud and precipitation microphysics. *Journal of Advances in Modeling Earth Systems*, 12, e2019MS001689. Available from: <https://onlinelibrary.wiley.com/doi/10.1029/2019MS001689>
- Petters, M.D. & Kreidenweis, S.M. (2007) A single parameter representation of hygroscopic growth and cloud condensation nucleus activity. *Atmospheric Chemistry and Physics*, 7, 1961–1971 <https://acp.copernicus.org/articles/7/1961/2007/>
- Pinsky, M., Khain, A. & Shapiro, M. (2001) Collision efficiency of drops in a wide range of Reynolds numbers: Effects of pressure on spectrum evolution. *Journal of the Atmospheric Sciences*, 58, 742–764. Available from: [https://doi.org/10.1175/1520-0469\(2001\)058<0742:CEODIA>2.0.CO;2](https://doi.org/10.1175/1520-0469(2001)058<0742:CEODIA>2.0.CO;2)
- Pruppacher, H. & Klett, J. (2010) *Microphysics of clouds and precipitation*. Atmospheric and Oceanographic Sciences Library, Vol. 18. Dordrecht: Springer Netherlands. Available from: <http://link.springer.com/10.1007/978-0-306-48100-0>
- Richter, D.H., MacMillan, T. & Wainwright, C. (2021) A Lagrangian cloud model for the study of marine fog. *Boundary-Layer Meteorology*, 181, 523–542. Available from: <https://doi.org/10.1007/s10546-020-00595-w>
- Schwenkel, J. & Maronga, B. (2019) Large-eddy simulation of radiation fog with comprehensive two-moment bulk microphysics: Impact of different aerosol activation and condensation parameterizations. *Atmospheric Chemistry and Physics*, 19, 7165–7181.
- Schwenkel, J. & Maronga, B. (2020) Towards a better representation of fog microphysics in large-eddy simulations based on an embedded Lagrangian cloud model. *Atmosphere*, 11, 466. Available from: <https://www.mdpi.com/2073-4433/11/5/466>
- Seifert, A., Nuijens, L. & Stevens, B. (2010) Turbulence effects on warm-rain autoconversion in precipitating shallow convection. *Quarterly Journal of the Royal Meteorological Society*, 136, 1753–1762. Available from: <https://onlinelibrary.wiley.com/doi/10.1002/qj.684>
- Shima, S., Kusano, K., Kawano, A., Sugiyama, T. & Kawahara, S. (2009) The super-droplet method for the numerical simulation of clouds and precipitation: A particle-based and probabilistic microphysics model coupled with a non-hydrostatic model. *Quarterly Journal of the Royal Meteorological Society*, 135, 1307–1320. Available from: <http://www.kemkes.go.id>, <https://onlinelibrary.wiley.com/doi/10.1002/qj.441>
- Spalart, P.R., Moser, R.D. & Rogers, M.M. (1991) Spectral methods for the Navier-Stokes equations with one infinite and two periodic directions. *Journal of Computational Physics*, 96, 297–324.
- Sweet, J., Richter, D.H. & Thain, D. (2018) GPU acceleration of Eulerian–Lagrangian particle-laden turbulent flow simulations. *International Journal of Multiphase Flow*, 99, 437–445. Available from: <https://linkinghub.elsevier.com/retrieve/pii/S0301932217306869>

- Unterstrasser, S., Hoffmann, F. & Lerch, M. (2017) Collection/aggregation algorithms in Lagrangian cloud microphysical models: Rigorous evaluation in box model simulations. *Geoscientific Model Development*, 10, 1521–1548. Available from: <https://gmd.copernicus.org/articles/10/1521/2017/>
- Wainwright, C., Chang, R.Y. & Richter, D. (2021) Aerosol activation in radiation fog at the Atmospheric Radiation Program Southern Great Plains Site. *Journal of Geophysical Research: Atmospheres*, 126, e2021JD035358. Available from: <https://onlinelibrary.wiley.com/doi/full/10.1029/2021JD035358>
- Wang, L.P. & Grabowski, W.W. (2009) The role of air turbulence in warm rain initiation. *Atmospheric Science Letters*, 10, 1–8. Available from: <https://onlinelibrary.wiley.com/doi/full/10.1002/asl.210>
- Zhang, X., Massoli, P., Quinn, P.K., Bates, T.S. & Cappa, C.D. (2014) Hygroscopic growth of submicron and supermicron aerosols in

the marine boundary layer. *Journal of Geophysical Research*, 119, 8384–8399. Available from: <https://onlinelibrary.wiley.com/doi/full/10.1002/2013JD021213>

How to cite this article: Rodriguez-Geno, C.F. & Richter, D.H. (2024) The role of collision and coalescence on the microphysics of marine fog. *Quarterly Journal of the Royal Meteorological Society*, 150(764), 4580–4593. Available from: <https://doi.org/10.1002/qj.4831>